First-Principle Calculations of Half-Metallic Double Perovskite La$_2BB'$O$_6$ ($B,B' = 3d$ transition metal)

Y. P. Liu[1], S. H. Chen[2], H. R. Fuh[3] and Y. K. Wang[4,*]

[1] *Department of Physics, National Taiwan Normal University, Taipei 116, Taiwan.*
[2] *Institute of Physics, Academia Sinica, Taipei 115, Taiwan.*
[3] *Graduate Institute of Applied Physics, National Taiwan University, Taipei 106, Taiwan.*
[4] *Center for General Education and Department of Physics, National Taiwan Normal University, Taipei 116, Taiwan.*

Abstract. In this paper, we present calculations based on density functional theory using generalized gradient approximation (GGA) in double perovskite structure La$_2BB'$O$_6$ ($B,B' = 3d$ transition metal) out of 45 (C_2^{10}) combinational possibilities. Considering 4 types of magnetic states, namely, ferromagnetic (FM), ferrimagnetic (FiM), antiferromagnetics (AF), and nonmagnetic (NM) with full structure optimization, 13 possible surviving, stable FM/FiM-HM materials containing 6 FM-HM materials (La$_2$ScNiO$_6$, La$_2$CrCoO$_6$, La$_2$CrNiO$_6$, La$_2$VScO$_6$, La$_2$VZnO$_6$, and La$_2$VNiO$_6$) and 7 FiM-HM materials (La$_2$VFeO$_6$, La$_2$ZnCoO$_6$, La$_2$TiCoO$_6$, La$_2$CrZnO$_6$, La$_2$CrMnO$_6$, La$_2$ScFeO$_6$, and La$_2$TiMnO$_6$) are found. Considering the correlation effect (GGA+U), there are 6 possible half-metallic stable, surviving (HM) materials containing 3 FM-HM materials (La$_2$ScNiO$_6$, La$_2$CrCoO$_6$, and La$_2$CrNiO$_6$) and 3 FiM-HM materials (La$_2$VFeO$_6$, La$_2$ZnCoO$_6$, and La$_2$TiCoO$_6$).

PACS: 75.10.Lp, 71.20.-b, 75.30.-m, 75.50.Ee

Key words: Half-metallic materials, double perovskites structure, first-principle density functional theory.

1 Introduction

In ordered double perovskites denoted as A$_2BB'$O$_6$ (A=alkaline-earth or rare-earth ion, B and B'=transition metal ion), the differences in the valance and size between the B

Corresponding author. Email addresses: `viva.guitarra@gmail.com` (Y. P. Liu), `chen_shao_hua197@yahoo.com.tw` (S. H. Chen), `c4491141@gmail.com` (H. R. Fuh), `kant@ntnu.edu.tw` (Y. K. Wang)

and B' cations are crucial for controlling the physical properties [1, 2]. Among them, Sr_2FeMoO_6 [3] has been discovered to possess colossal magneto resistance (CMR) at room temperature. The high transition temperature T_c and low field magnetoresistance indicate half-metallic (HM) behavior in this compound. In HM materials, there is a well-defined gap in the majority channel and a metallic behavior in the minor spin channel. Thus, HM materials have three properties: (1) quantization of the magnetic moment; (2) 100% spin polarization at the Fermi level; (3) zero spin susceptibility. Due to their single-spin charge carriers, HM materials can be used in creating computer memories, magnetic recordings, and so on.

This work searches for new HM materials in all the 45 (C_2^{10}) double pervoskite structure of $La_23d3d'O_6$ series, where $3d3d'$ pairs are combinations of all $3d$ transition elements. The research is based on the first-principle generalized gradient approximation (GGA) calculations, with the consideration of four types of magnetic states, namely, ferromagnetic (FM), ferrimagnetic (FiM), antiferromagnetics (AF), and nonmagnetic (NM), in ideal cubic structure ($Fm\bar{3}m$, No. 225). Up to 22 possible compounds were obtained from the first round of filtering calculation. After the structural optimization process and considering the energy difference between the 4 magnetic states, 13 possible FM/FiM-HM materials proved to be stable containing 6 FM-HM materials (La_2ScNiO_6, La_2CrCoO_6, La_2CrNiO_6, La_2VScO_6, La_2VZnO_6, and La_2VNiO_6) [27] and 7 FiM-HM materials (La_2VFeO_6, La_2ZnCoO_6, La_2TiCoO_6, La_2CrZnO_6, La_2CrMnO_6, La_2ScFeO_6, and La_2TiMnO_6). In transition metal oxides, the strong electron correlation systems need better description rather than GGA calculations. However, GGA calculations can be corrected using a strong-correlation correction called GGA(LDA)+U method. In the GGA+U process, U and J stand for Coulomb and exchange parameters, respectively, and the effective parameter $U_{eff} = U - J$ is adopted. In this paper, we used U instead of U_{eff} for simplicity. Our result matched that of a previous study, which indicates that La_2NiFeO_6 [4] and La_2ZnRuO_6 [5] are HM materials upon which La_2NiFeO_6 needs to base the GGA+U calculations on; La_2VMnO_6 [6] and La_2VCuO_6 [7, 8] are half-metallic antiferromagnetics (HM-AFM) where La_2VMnO_6 needs to go through for full structural optimization calculation; and La_2NiMnO_6 [9–11] is a ferromagnetic insulator (FM-Is) material. Based on our result, La_2ScNiO_6, La_2CrCoO_6, and La_2CrNiO_6 are half-metallic ferromagnetic (FM-HM) compounds and La_2VFeO_6, La_2ZnCoO_6, and La_2TiCoO_6 are half-metallic ferrimagnetic (FiM-HM) materials.

2 Computational method

The theoretical research was based on density functional theory (DFT) [12], and using GGA [13] to approach the exchange-correlation potential. The structural optimization (i.e., relaxation for both lattice constants and atomic positions) were carried out using the full-potential projector augmented wave (PAW) [14] method and the conjugate-gradient (CG) method as implemented in the VASP code [15, 16], which is fast and efficient. To

obtain the electronic structure more accurately, the optimized VASP structure is used as input for the highly accurate full-potential linearized augmented plane wave (FLAPW) method [17,18] as implemented in the WIEN2K package [19]. The wave function, charge density, and potential were expanded in terms of spherical harmonics inside the muffin-tin spheres. Outside the muffin-tin spheres, they were expanded in terms of the augmented plane wave. The result (both in energy and magnetic properties) all matched qualitatively from both codes.

In the structural optimization process of the VASP code, the plane wave cutoff energy was set to 450 eV, and $8 \times 8 \times 6 k$-points grids were set in the Brillouin zone. The energy convergence criterion was 10^{-5} eV. The theoretical equilibrium structure was obtained when the forces and stresses acting on all the atoms were less than 0.01 eV/Angst and 1.2 kBar, respectively. In the self-consistent process of WIEN2K package, the cutoff angular momentum (L_{max}) was set to 10 for the wave functions and 6 for the charge density and potential. The number of augmented plane waves was about 120 per atom (i.e., $R_{max} \times K_{max} = 6$). The improved tetrahedron method was used for the Brillouin zone integration [20]. Up to 120, 163, and 144 k-points numbers were used in the irreducible Brillouin zone wedge for the $Fm\bar{3}m$, $14/mmm$, and $P4/mmm$ structures, respectively. The muffin-tin sphere radii were set to 2.5 a.u. for La, 2.0 a.u. for $3d$ materials, and 1.4 a.u. for O.

The on-site electron correlation correction (GGA+U) [21–25] scheme was also considered for describing strong electron correlation systems, such as transition metal oxides. In the GGA+U calculation, U and J stand for Coulomb and exchange parameters, respectively, and the effective parameter $U_{eff} = U - J$ is adopted. In this paper, we used U instead of U_{eff} for simplicity. In $3d$ transition metals, we selected the near-maximum values from the reasonable range of U [26]. For example, the range U for Fe is 3.0 eV to 6.0 eV. The value of 5.0 is used in the calculation. The detail U values are listed in Table 1. There are four magnetic phases in the ordered double perovskite structure La$_2$$BB'O_6$ (Fig. 1), denoted as FM, FiM, AF, and NM states. The spin state of the two B and B' ions dominates the magnetic state of the material.

3 Result and discussion

3.1 Magnetic stable phase and crystal structures

Four magnetic states are considered in the ordered double perovskite structure A$_2$$BB'O_6$ denoted as nonmagnetic (NM), ferromagnetic (FM), ferrimagnetic (FiM), and antimagnetic (AF) states. Each state is controlled by the spin state of the two B and B' ions. B and B' ions have their own spin state, that is, $(B,B,B',B') = (m,m,m',m') =$ FM or $(m,m,-m',-m') =$ FiM, which can probably lead us to the assumption of the HM state. The AF state occurs when the B and B' ions along the chain are ferromagnetically polarized but the neighbor chain is antiferromagnetic-coupled (i.e., (B,B,B',B') is $(m,-m,m',-m')$ in the superlattice). In AF state, no HM state exists because the total

Table 1: Calculated physical properties of the possible FM/FiM-HM materials in double perovskite (La$_2BB'$O$_6$) structure in the full structural optimization calculation of GGA($+U$).

Materials		Spin magnetic moment (μ_B/f.u.)			d orbital electrons ↑/↓		$N(E_F)$	Band gap	ΔE=FM-AF
La$_2[BB']$O$_6$	$U(B,B')$	m_B	$m_{B'}$	m_{tot}	B	B'	state/eV/f.u.	eV	meV
ScNi	$U(0,0)$	0.045	0.788	1.000	0.368/0.328	4.251/3.465	↑2.218	↓1.497	-0.1
	$U(2.6)$	0.027	1.255	1.000	0.351/0.318	4.479/3.234	↑1.779	↓3.211	-1.1
CrCo	$U(0,0)$	2.410	0.150	3.000	2.966/0.576	3.446/3.291	↑5.081	↓0.762	-18.4
	$U(3,6)$	2.527	-0.019	3.000	3.010/0.505	3.327/3.341	↑1.365	↓2.471	5.7
CrNi	$U(0,0)$	2.048	1.393	4.000	2.373/0.723	4.578/3.189	↑9.547	↓1.007	-51.8
	$U(3.6)$	2.034	1.707	4.000	2.698/0.695	4.739/3.039	↑7.609	↓3.293	5.3
VSc	$U(0,0)$	1.416	0.048	2.000	1.938/0.535	0.363/0.314	↑4.112	↓3.238	-44.0
	$U(3.2)$	1.503	0.038	2.000	1.973/0.484	0.343/0.306	↑4.254	↓3.238	167.1
VZn	$U(0,0)$	0.824	0.001	1.000	1.594/0.779	4.819/4.817	↑6.987	↓2.259	-48.9
	$U(3.7)$	0.879	0.001	1.000	1.600/0.730	4.847/4.845	↑6.307	↓2.934	249.2
VNi	$U(0,0)$	0.930	1.552	3.000	1.649/0.745	4.666/3.119	↑7.301	↓1.116	-38.4
	$U(3.6)$	0.973	1.731	3.000	1.644/0.691	4.746/3.024	↑6.932	↓3.265	275.9
VFe	$U(0,0)$	-0.929	3.600	3.000	0.748/1.681	4.581/1.007	↓3.470	↑0.978	-232.9
	$U(3.5)$	-1.254	4.001	3.000	0.736/1.848	4.708/0.594	↓3.627	↑2.313	-107.8
ZnCo	$U(0,0)$	-0.011	0.794	1.000	4.799/4.809	3.712/2.923	↓7.639	↑0.871	-47.1
	$U(7.6)$	-0.004	0.574	1.000	4.840/4.841	3.606/3.035	↓9.195	↑1.823	-54.1
TiCo	$U(0,0)$	-0.006	0.913	1.000	0.740/0.673	3.863/2.955	↑2.134	↓0.816	1.8
	$U(2.6)$	0.085	1.075	1.000	0.724/0.637	3.970/2.904	↑1.958	↓1.932	-4.4
CrZn	$U(0,0)$	1.765	-0.004	2.000	2.585/0.837	4.816/4.817	↑6.283	↓2.177	-53.3
	$U(3.7)$	1.882	-0.002	2.000	2.629/0.765	4.846/4.845	↑6.104	↓3.020	178.8
CrMn	$U(0,0)$	-2.202	3.241	1.000	0.685/2.869	3.873/0.662	↑1.887	↓0.925	-3.9
	$U(3.5)$	-2.384	3.622	1.000	0.590/2.952	4.040/0.451	↑0.892	↓1.769	201.6
ScFe	$U(0,0)$	-0.018	0.923	1.000	0.335/0.351	3.290/2.373	↓5.663	↑1.551	-74.3
	$U(2.5)$	-0.018	0.900	1.000	0.319/0.336	3.267/2.373	↓5.621	↑2.803	763.8
TiMn	$U(0,0)$	-0.301	1.329	1.000	0.580/0.875	2.984/1.665	↓3.621	↑1.034	-259.8
	$U(2.5)$	-0.453	1.640	1.001	0.497/0.944	3.101/1.473	↑↓0.045/3.317	~↑2.830	1396.1

DOS of spin-up and spin-down is symmetrical, which results from the induced equivalence in the charges: $Q\uparrow[B(B')]=Q\downarrow[B(B')]$. For NM state, no spin-polarized calculation and no magnet properties exist. The result shows that the spin-polarized calculations of total energies are always lower than that without spin polarization. To guarantee the accuracy of the calculation result, full structural optimization with higher convergence criteria was also performed.

In full structural optimization, the ideal cubic perovskite structure ($Fm\bar{3}m$, No. 225) reduces to tetragonal structure ($I4/mmm$, No. 139) in the FM or FiM state, except La$_2$TiCoO$_6$, which is in the space grope $Fmmm$, No. 69. In Fig. 1, the ideal cubic double perovskite structure ($Fm\bar{3}m$) that can be described by a faced-centered cubic (fcc) lattice with lattice constant $2a$ is shown. The $B(B')$ ion is coordinated by $B'(B)$ ion using a O ion in the middle as an intermediate and the length of B-O and B'-O is equal. After relaxation, both lattice constants and atomic positions reduce the ideal cubic (space group $Fm\bar{3}m$) structure to tetragonal (space group $I4/mmm$) structure, except La$_2$TiCoO$_6$. The tetragonal structure has two unequal types of O atoms shown in Table 2. There are two O$_1$ atoms located on the z-axis, with $B(B')$ and $B'(B)$ atoms in between and four O$_2$ atoms
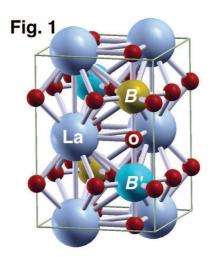
Figure 1: An ideal ordered double perovskite structure $La_2BB'O_6$. For FiM state, the spin state of (B,B,B',B') is $(+,+,-,-)$. For AF state, the spin state of (B,B,B',B') is $(+,-,+,-)$.

located on the same plane as the B and B' atoms (Fig. 1 and Table 2). The structure of La_2TiCoO_6 (space grope *Fmmm*, No. 69) has three unequal types of O atoms, as shown in Table 2. The pairs of O_1 to O_3 atoms lay on the z-axis, y-axis, and x-axis, each with different bond lengths. Each position component is very close to $0.25a$ (lattice constant) which is very close to the ideal cubic. Although the lattice constant and bond length changes after full structural optimization, the angle of the B-O-B' still remains at $180°$. The symmetry reduction is rather minor, i.e., the c/a ratio is very close to the ideal value $\sqrt{2}$. In the AF state, the initial tetragonal structure ($P4/mmm$, No. 123) remains in the same space group after full structural optimization.
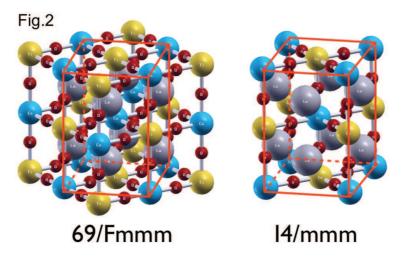

Figure 2: Double perovskite structure in space group $69/Fmmm$ and $I4/mmm$.

Table 2: Structural parameters of the possible FM/FiM-HM materials in the fully optimized structure ($I4/mmm$, No. 139), where La(x,y,z)=(0,0.5,0.75), $B(x,y,z)$=(0,0,0), and $B'(x,y,z)$=(0,0,0.5), except La$_2$TiCoO$_6$, is in space group ($Fmmm$, No. 69) where La(x,y,z)=(0.25,0.25,0.25), $B(x,y,z)$=(0,0,0), and $B'(x,y,z)$=(0,0,0.5).

La$_2[B(B')]$O$_6$	ScNi	CrCo	CrNi	VFe	ZnCo	TiCo
a	5.5842	5.4461	5.4735	5.4464	5.4766	5.5097
c/a	1.4142	1.4142	1.4142	1.4142	1.4142	1.4142
V_0(Å^3/f.u.)	123.13	114.22	115.95	114.24	116.15	118.27
O$_1 x$	0	0	0	0	0	0
O$_1 y$	0	0	0	0	0	0
O$_1 z$	0.2570	0.2522	0.2467	0.2450	0.2587	0.2500
O$_2 x$	0.2431	0.2479	0.2533	0.2549	0.2414	0
O$_2 y$	0.2431	0.2479	0.2533	0.2549	0.2414	0.2500
O$_2 z$	0.5	0.5	0.5	0.5	0.5	0.5000
O$_3(x,y,z)$	-	-	-	-	-	(0.2500,0,0)

Twenty-two possible HM materials were found in the first round of searching, where FLAPW method is used to calculate the self-consistent electronic structure of all La$_2 3d3d'$O$_6$ series (45 compounds) in the ideal cubic structure ($Fm\bar{3}m$, No. 225, lattice constant a=7.8Å). After full structural optimization calculation, 20 possible HM materials are left. However, only La$_2$VMnO$_6$ [6] and La$_2$VCuO$_6$ [7,8] are half-metallic antiferromagnetic (HA-AFM) materials. After comparing the total energies between the four magnetic states, 13 possible FM/FiM-HM materials containing 6 FM-HM materials (La$_2$ScNiO$_6$, La$_2$CrCoO$_6$,La$_2$CrNiO$_6$,La$_2$VScO$_6$, La$_2$VZnO$_6$, and La$_2$VNiO$_6$) [27] and 7 FiM-HM materials (La$_2$VFeO$_6$, La$_2$ZnCoO$_6$, La$_2$TiCoO$_6$, La$_2$CrZnO$_6$, La$_2$CrMnO$_6$, La$_2$ScFeO$_6$, and La$_2$TiMnO$_6$) are found to be stable. Strong-correlation correction (GGA+U) scheme is considered for the d orbitals with the U values denoted as ($U_B, U_{B'}$) for transition metals. Considering strong-correlation correction (GGA+U), the energy difference of FM state and AF state of La$_2$VScO$_6$, La$_2$VZnO$_6$, La$_2$VNiO$_6$, La$_2$CrZnO$_6$, La$_2$CrMnO$_6$, La$_2$ScFeO$_6$, and La$_2$TiMnO$_6$ shows that AF state is more stable than FM state for over 100 meV per formula unit (f.u.). Thus, this paper will focus on the six possible candidates of FM/FiM-HM materials.

However, for La$_2$ScNiO$_6$ and La$_2$TiCoO$_6$, the energy difference between AF and FM(FiM) states is quite small (only below 5 meV/f.u., Table 1); thus, it is difficult to ascertain whether the small energy difference lies in the error bar. That is, it is possible that the two magnetic states (AF and FM/FiM) almost degenerate. In other words, the coexistence of the AF and FM/FiM states can be expected.

3.2 FM-HM compounds: La$_2$ScNiO$_6$, La$_2$CrCoO$_6$, and La$_2$CrNiO$_6$

According to the result, all three compounds La$_2$ScNiO$_6$ (LSNO), La$_2$CrCoO$_6$ (LCCO), and La$_2$CrNiO$_6$ (LCNO) converge from FiM state to FM state in structural optimization. Thus, the density of states (DOS) are presented in FM state (Fig. 3). In GGA calculation

process, the materials (LSNO, LCCO, and LCNO) appear to be half-metallic with total magnetic moments of 1.0, 3.0, and $4.0\mu_B$ with energy gap of 1.50, 0.76, and 1.01 eV at the spin-down channel, respectively.

In LSNO, Ni(Co) $3d$ and O $2p$ orbital hybridize with each other overall, and spin splitting near the Fermi level (E_F) causes the HM property. O $2p$ and Sc $3d$ orbitals hybridize at the same energy region as the Ni $3d$ orbital. The spin splitting of Ni e_g states at E_F drags the Sc e_g orbital together through the Ni_{eg}-O_{2p}-Sc_{eg} hybridization and double exchange interaction, and pushes the spin-down states above E_F, which creates an energy gap and induces a weak magnetic moment ($0.045\mu B$) for Sc. The total charge population of d orbital for Sc and Ni are 0.70 and 7.72, respectively, which gives the valence states of $Sc^{+2.30}(3d^{0.70})(S=0)$ and $Cr^{+2.28}(3d^{7.72})(S=1/2)$. When non-spin magnetic elements sit between spin magnetic elements, Terakura et al. [28] proposed the FiM stabilization mechanism, which indicates that the main reasons for the half metallicity are p-d hybridization and double exchange. The spin-polarized magnetic elements are denoted as d-states, and the nonmagnetic elements located between the spin-split d-states are denoted as p-state while E_F goes through the p band. With the effect of p-d hybridization, the d-state pushes the p-state upward (downward) at the spin down (up) channel, which will separate the E_F in different spin channels, resulting in unequal E_F between two spin states. To keep the E_F similar in both spin states, a number of electrons will switch spin states that move non-spin magnetic elements to contribute negative moments and stabilize the FiM state. If p-d hybridization is strong enough to push the p-state above the E_F at the spin up channel while the band extends at the spin down channel with the E_F lying with the double exchange effect, half metallicity can be obtained. For LCCO, the Cr $3d$ band represents the spin-split d-state spin magnetic elements and Co $3d$ band stands for the p-state non-spin magnetic elements. The total charge population of d orbital for Cr and Co is 3.54 and 6.74, respectively. These values give the valence states of $Cr^{+2.46}(3d^{3.54})(S=3/2)$ and $Cr^{+2.26}(3d^{6.74})(S=0)$. For LCNO, the Cr t_{2g} and Ni e_g orbitals dominate the metallic property in the spin-up channel, and spin splitting causes an energy gap in the spin-down channel. Thus, they each have strong magnetic moments of 2.048 and $1.393\mu B$ for Co and Ni. There is a strong spin splitting for Cr t_{2g} and Ni e_g at E_F. The spin-down states are pushed up above E_F and gives an energy gap of 1.0 eV. The narrow band at E_F indicates the highly localized electrons, which repulse the Ni t_{2g} orbitals downward at about -1 eV to -2 eV. The total charge population of d orbital for Cr and Ni are 3.46 and 7.77, respectively. These values give the valence states of $Cr^{+2.54}(3d^{3.46})(S=1)$ and $Ni^{+2.23}(3d^{7.77})(S=1)$.

Choosing an appropriate U in finding new compounds where the value of U is often based on the result of experiment is difficult. The effect of the electron correlation correction will enhance the localization of the $3d$ orbitals and push unoccupied states to higher energy level, thus increasing the magnetic moment and energy gap. While considering the electron correlation correction effect (GGA+U), the total magnetic moment still remains the same, but the energy gap reaches 3.21, 2.47, and 3.29 eV for LSNO, LCCO, and LCNO, respectively (Fig. 4). In LSNO, the magnetic moment of Ni is $1.255\mu B$. How-
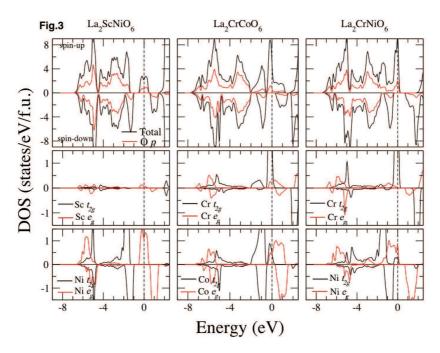
Figure 3: Calculated total, spin, and site-decomposed density of states of La_2ScNiO_6, La_2CrCoO_6, and La_2CrNiO_6 in GGA process.
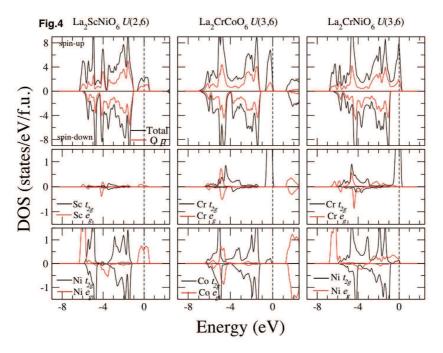

Figure 4: Calculated total, spin, and site-decomposed density of states of La_2ScNiO_6, La_2CrCoO_6, and La_2CrNiO_6 in GGA+U process.

ever, the total magnetic moment is $1.000\mu B$. Thus, some small magnetic moments exist (about $-0.040\mu B$) in each O atom and interstitial space. For LCCO, the e_g orbitals have been pushed up but the t_{2g} orbital on the spin-up channel near the Fermi level remains at the same energy region. The spin-down channel remains in metal form about 1.365 stats/eV/f.u. at the Fermi level. When the value of U becomes larger, a ferromagnetic insulator (FM-Is) material can be obtained. For LCNO, the orbitals above E_F are pushed up, but the e_g orbital on the spin-up channel at the Fermi level remains at the same energy region.

3.3 FiM-HM compounds: La$_2$VFeO$_6$, La$_2$ZnCoO$_6$, and La$_2$TiCoO$_6$

During the research, La$_2$VFeO$_6$ (LVFO), La$_2$ZnCoO$_6$ (LZCO), and La$_2$TiCoO$_6$ (LTCO) indicated that the FM and FiM states all converged to FiM state in structural optimization. Therefore, the density of states (DOS) is presented in FiM state (Fig. 5). In GGA calculation, the FiM compounds (LVFO, LZCO, and LTCO) appeared to be half-metallic with total magnetic moments of 3.0, 1.0, and $1.0\mu B$ and energy gaps of 0.98, 0.87, and 0.82 eV at the spin-up, spin-up, and spin-down channel, respectively.

In LVFO, the V t_{2g} and Fe t_{2g} orbitals dominate the metallic property in the spin-up channel, and spin splitting causes an energy gap in the spin-down channel. In LCNO, both transition metal ions have full orbital spin polarization, which produces two strong local magnetic moments of 0.93 and $3.60\mu B$ for V and Fe, respectively. In the spin-up channel, the Fe $3d$ states are all below E_F and give the repulsion to V t_{2g} orbitals. They opens an energy gap at the spin-up channel. With the double exchange interaction and V_{t2g}-O_{2p}-Fe_{eg} hybridization at the spin-down channel, the HM characteristic appears. Compared with LCNO (Fig. 3), the $3d$ orbitals of Cr and Ni are symmetric (i.e., the band of the spin-up channel is lower than that of the spin-down channel). In LVFO (Fig. 5), the Fe $3d$ band of the spin-up channel is higher than that of the spin-down channel, and the V $3d$ band has the opposite behavior. Thus, V $3d$ orbitals are anti-symmetric against Fe, and the FiM phase can be obtained. The total charge population of d orbital for V and Fe is 2.43 and 5.59, respectively, which gives the valence states of $V^{+2.57}(3d^{2.43})(S=-1/2)$ and $Fe^{+2.41}(3d^{5.59})(S=2)$. For LZCO, the energy split of the t_{2g} and e_g orbital indicates that the structure distortion is strong. Co $3d$ and O $2p$ orbital hybridization occurs mainly in the energy region -7.0 eV to -3.8 eV and -3.2 eV to 0.5 eV. The total magnetic moment originates from Cr because the orbitals for Zn below E_F are fully symmetrical. Likewise, in LSNO, the spin splitting of Co t_{2g} with E_F lying on the spin down orbital results in half metallicity. With the double exchange interaction and Zn_{eg}-O_{2p}-Co_{t2g} hybridization, a weak magnetic moment of $-0.011\mu B$ is induced for Zn. The total charge population of d orbital for Zn and Co is 9.61 and 6.64, respectively, which gives the valence states of $Zn^{+2.39}(3d^{9.61})(S=0)$ and $Co^{+2.36}(3d^{6.64})(S=1/2)$. For LTCO, because the crystal is very close to the cubic structure, the energy splitting between e_g and t_{2g} orbitals can hardly be found. Thus, the hybridization between the [Co $3d$, O $2p$] orbitals and [Ti $3d$, O $2p$] orbitals are perfectly matched at all energy regions. The spin splitting of Co $3d$ orbitals
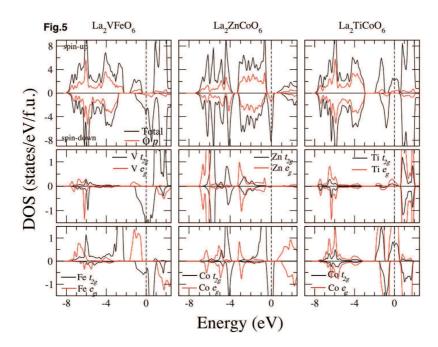
Figure 5: Calculated total, spin, and site-decomposed density of states of La$_2$VFeO$_6$, La$_2$ZnCoO$_6$, and La$_2$TiCoO$_6$ in GGA process.
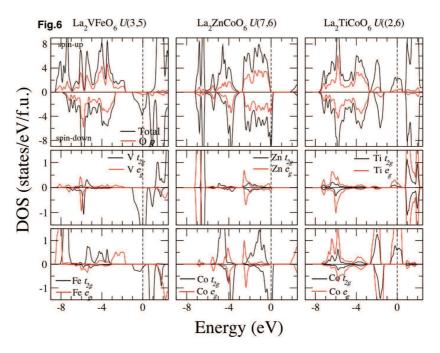

Figure 6: Calculated total, spin, and site-decomposed density of states of La$_2$VFeO$_6$, La$_2$ZnCoO$_6$, and La$_2$TiCoO$_6$ in GGA+U process.

with the E_F located on the spin-up state results in half metallicity of the compound. The Co $3d$ orbitals below E_F at the energy region of -1 to -2 are repulsed by the extending Co $3d$ orbitals on the E_F. With the Ti_{3d}-O_{2p}-Co_{3d} hybridization and double exchange interaction at the spin-up channel, a weak magnetic moment of $-0.006\mu B$ is induced for Ti. The total charge population of d orbital for Ti and Co is 1.41 and 6.82, respectively. This value gives the valence states of $Ti^{+2.59}(3d^{1.41})(S=0)$ and $Co^{+2.18}(3d^{6.82})(S=1/2)$. For LZCO and LTCO, because the induced local magnetic moment for Zn and Ti are weak (less than $0.02\mu B$), the magnetic moment can be regarded as zero. Their half metallic mechanisms are similar to LSNO, so we can also count them (LZCO and LTCO) as FM-HM.

Considering the electron correlation correction effect (GGA+U), the total magnetic moment still remains the same, but the energy gap reaches 2.31, 1.82, and 1.93 eV for LVFO, LZCO, and LTCO, respectively (Fig. 6). For LVFO, the e_g orbital at spin-up channel below the E_F moves to a lower energy region that opens a larger gap of 2.31 eV. The t_{2g} orbital remains at the same energy region but becomes more localized. For LZCO, the Co e_g orbitals above E_F are pushed up, but the t_{2g} orbital on the spin-up channel near the Fermi level remains at the same energy region. The spin-splitting of the Co t_{2g} orbitals extend into the lower-energy region, whereas other orbitals have more spin symmetry. For LTCO, the Co e_g orbital at the spin-up channel separates near the E_F, but the Ti e_g orbital remains at the same energy region.

4   Conclusions

Based on DFT with GGA approaches, the calculation results of the $La_2 3d3d'O_6$ series out of 45 (C_2^{10}) combinations are presented in this work. After full-structural optimization and comparison of the energy difference between each of the 4 types of magnetic states (FM, FiM, AF, and NM), 13 possible surviving, stable FM/FiM-HM materials containing 6 FM-HM materials (La_2ScNiO_6, La_2CrCoO_6, La_2CrNiO_6, La_2VScO_6, La_2VZnO_6, and La_2VNiO_6) and 7 FiM-HM materials (La_2VFeO_6, La_2ZnCoO_6, La_2TiCoO_6, La_2CrZnO_6, La_2CrMnO_6, La_2ScFeO_6, and La_2TiMnO_6) are found. By incorporating a strong-correlation correction (GGA+U), 6 possible half-metallic stable, surviving (HM) materials containing 3 FM-HM materials (La_2ScNiO_6, La_2CrCoO_6, and La_2CrNiO_6) and 3 FiM-HM materials (La_2VFeO_6, La_2ZnCoO_6, and La_2TiCoO_6) are found. LSNO, LCCO, LZCO, and LTCO can be regard as couples with one strong magnetic element and one weak magnetic element, that is, the effect of p-d hybridization. The fully spin-polarized strong spin magnetic elements induce the weak magnetic element to slightly increase the positive (negative) magnetic moment; thus, it is regarded as the main cause of HM properties. For LCNO and LVFO, the spin polarization is strong for each $3d$ orbital of transition metal ions. Consequently, the local magnetic moments for the transition metal ions cannot be ignored. The half-metallic characteristics are dominated by spin splitting and double exchange interaction of each material. Hopefully, this work offers more candidates and encourages further experimental research on HM materials.

Acknowledgments

References

[1] F. Galasso, Inorg. Chem. 2 (1963) 482.
[2] T. Nakamura, J. H. Choy, J. Solid State Chem. 20 (1977) 233.
[3] K.-I. Kobayashi et al., Nature 395 (1998) 677.
[4] S. Li et al., J. Phys. Chem. C 114 (2010) 16710.
[5] W. Song et al., Chem. Phy. Letters 486 (2010) 27.
[6] S. H. Chen et al., Physica B 406 (2011) 2783-2787.
[7] Y. K. Wang, P. H. Lee and G. Y. Guo, Phys. Rev. B 80 (2009) 224418.
[8] W. E. Pickett, Phys. Rev. B 57 (1998) 10613.
[9] H. Das et al., Phys. Rev. L100 (2008) 186402.
[10] S.F. Matar et al., J. Magn. Magn. Mater. 308 (2007) 116-119.
[11] N. S. Rogado et al., Adv. Mater. 17 (2005) 2225-2227.
[12] P. Hohenberg and W. Kohn, Phys. Rev. 136, B864 (1964); W. Kohn and L. J. Sham, Phys. Rev. 140 (1965) A1133.
[13] J. P. Perdew, K. Burke and M. Ernzerhof, Phys. Rev. Lett. 77 (1996) 3865.
[14] P. E. Blöchl, Phys. Rev. B 50 (1994) 17953.
[15] G. Kresse and J. Hafner, Phys. Rev. B 48 (1993) 13115.
[16] G. Kresse and J. Furthmüller, Comput. Mater. Sci. 6 (1996) 15; Phys. Rev. B 54 (1996) 11169.
[17] O. K. Andersen, Phys. Rev. B 12 (1975) 3060.
[18] D. D. Koelling and G. O. Arbman, J. Phys. F: Met. Phys. 5 (1975) 2041.
[19] P. Blaha, K. Schwarz, G. K. H. Madsen, D. Kvasnicka and J. Luitz, wien2K, An Augmented Plane Wave Local Orbitals Program for Calculating Crystal Properties Techn. University Wien, Austria, 2002.
[20] P. E. Blöchl, O. Jepsen and O. K. Andersen, Phys. Rev. B 49 (1994) 16223.
[21] V. I. Anisimov, J. Zaanen and O. K. Andersen, Phys. Rev. B 44 (1991) 943.
[22] A. I. Lichtenstein, V. I. Anisimov and J. Zaanen, Phys. Rev. B 52 (1995) R5467.
[23] V. I. Anisimov, F. Aryasetiawan and A. I. Lichtenstein, J. Phys.: Condens. Matter 9 (1997) 767.
[24] H.-T. Jeng, G. Y. Guo and D. J. Huang, Phys. Rev. Lett. 93 (2004) 156403.
[25] X. F. Jiang and G. Y. Guo, Phys. Rev. B 70 (2004) 035110.
[26] I. V. Solovyev, P. H. Dederichs and V. I. Anisimov, Phys. Rev. B. 50 (1994) 16861.
[27] K. L. Holman et al., Journal of Solid State Chemistry 180 (2007) 75-83.
[28] K. Terakura, Z. Fang and J. Kanamori, Journal of Physics and Chemistry of Solids 63 (2002) 907-912.